A 3D Reactive Collision Avoidance Algorithm for Nonholonomic Vehicles

Martin S. Wiig[1,2], Kristin Y. Pettersen[1,2] and Thomas R. Krogstad[2]

***Abstract*— This paper presents a 3D reactive collision avoidance algorithm for vehicles with nonholonomic constraints. The algorithm steers the heading and pitch angle of the vehicle in order to maintain a constant avoidance angle to the obstacle, thus ensuring a safe collision avoidance maneuver. The flexibility provided by moving in three dimensions is utilized by choosing an optimal pair of safe pitch and heading angles for avoidance. Furthermore, the algorithm incorporates limits on the allowed pitch angle, which are often present in practical scenarios. The collision avoidance property is mathematically proved, and the analysis is validated by several numerical simulations.**

I. INTRODUCTION

For unmanned vehicles operating without manned supervision, it is of vital importance to be able to react quickly to detected obstacles. This is particularly true for vehicles operating in 3D, such as unmanned aerial vehicles (UAVs), which can fly at high speed, or for autonomous underwater vehicles (AUVs), which operate in mostly unknown environments often characterized by difficult sensing conditions.

Reviews of different collision avoidance (CA) approaches in 2D are given in [1] and [2]. The different approaches can generally be divided into two groups [3]; motion planning algorithms and reactive algorithms. The general motion planning problem with bounded velocities and multiple obstacles has been shown to be NP-hard [4], and can be computationally expensive. This can particularly be a problem in 3D, where the added dimension extends the planning complexity significantly. Reactive algorithms therefore seem promising in such scenarios.

The artificial potential field approach for obstacle avoidance has been in much use since it was proposed in [5]. There are, however, some stability issues identified by [6], which the vector field histogram [7] seeks to counter by choosing a safe direction from a polar histogram of merged sensor measurements. Another potential field approach is the navigation vector field [8], where local minima are avoided by directly creating a gradient field with this in mind. The potential field methods do not inherently consider vehicle dynamics, and the performance of the algorithm on vehicles with nonholonomic constraints is rarely analyzed. An example of a 2D algorithm incorporating vehicle dynamics and constraints is the dynamic window algorithm [9], [10], which searches through a set of valid vehicle trajectories to find a safe control input.

In [11], a reactive algorithm employing a dipolar navigation function resembling the artificial potential field is used. The navigation function is generated so that there is a single minimum at the target, and maxima at the obstacles. The algorithm provably makes the vehicle reach the target position while avoiding obstacles. However, there is an underlying assumption that the vehicle is able to follow the integral curves. Furthermore, actuator constraints are not included, nor is there any analysis on the behavior of the vehicle forward speed. In particular, it is not guaranteed that the forward speed is always positive.

The velocity obstacle [12] and collision cone [13] approaches deal with moving obstacles in the plane. Several extensions have been made to the velocity obstacle approach to consider acceleration constraints and nonholonomic constraints [14], [15]. The velocity obstacle approach has been used with much success. However, for vehicles with very limited speed envelopes, it can become too restrictive.

A 3D extension to the velocity obstacle approach is proposed for a UAV scenario in [16] and [17]. The problem of selecting a reachable velocity is elegantly solved by dividing the 3D space into a discrete set of planes, and examining each plane. Hence, the vehicle can choose the best velocity across multiple planes according to some criterion. The dynamics of a vehicle controlled by the algorithm is, however, not analyzed, and there is a concern with oscillations when switching between the different avoidance planes. Furthermore, the problems related to limited speed envelopes remains unsolved.

Another reactive algorithm for nonholonomic vehicles is presented in [18], where a constant avoidance angle is maintained between the vehicle heading and the tangent from the vehicle to the obstacle. The algorithm has a low computational complexity and limited vehicle sensing requirements. It is mathematically proved that the vehicle avoids obstacles moving with constant velocity. There is, however, a singularity in the algorithm for certain obstacle speeds, and the algorithm can make the vehicle almost stop. The latter is unfortunate for vehicles such as fixed-wing aircraft, which has a limited flight envelope.

The algorithm in [18] is extended to 3D in [19]. Here, the vehicle is made to move in a plane created from the vehicle's velocity vector and the obstacle center. The 2D algorithm of [18] is then implemented in this plane. The approach is an

This work was partly supported by the Research Council of Norway through the Centres of Excellence funding scheme, project no. 223254 - NTNU AMOS

[1]Centre for Autonomous Marine Operations and Systems (NTNU AMOS), Department of Engineering Cybernetics, Norwegian University of Science and Technology, 7491 Trondheim, Norway. Martin.Wiig@itk.ntnu.no

[2]Norwegian Defence Research Establishment (FFI), P.O. Box 25, N-2027 Kjeller, Norway.

intuitive extension from 2D to 3D, and it is proved that the algorithm is safe. However, the algorithm does not fully make use of the flexibility offered by moving in three dimensions, and it is not possible to limit vehicle pitch. Furthermore, as with [18], the algorithm can make the vehicle speed close to zero, which is particularly unfortunate in three dimensions.

The algorithm proposed by [20] extends the work of [18] to accommodate vehicles that must move within a limited speed envelope, and also avoids the singularity in the analysis. Both [20] and [18] consider kinematic vehicles, while in [21] the algorithm is extended to a marine vehicle with underactuated dynamics.

The main contribution of this paper is a 3D reactive CA algorithm for nonholonomic vehicles. The algorithm is an extension of the 2D algorithm in [20]. The algorithm steers the heading and pitch angle of the vehicle, and is able to find safe angles for any given vehicle forward speed. It can thus accommodate vehicles with a limited speed envelope, which is particularly relevant in 3D scenarios for vehicles such as UAVs and AUVs. To show the applicability to such vehicles, we apply the algorithm to a vehicle that is restricted to keep a constant forward speed. The algorithm can also be used on vehicles without such restrictions, and will then give a large amount of flexibility in designing the desired speed trajectory.

We introduce an extended 3D vision cone, which is used to define the set of safe heading and pitch angles, and to define the criterion for transition between guidance mode and CA mode. Unlike the 2D case, where the vehicle can choose between two safe heading angles from the algorithm, we have a continuum of safe heading and pitch angles in the 3D scenario. We will use this flexibility to define a general optimization criterion for selecting an optimal pair of heading and pitch angles. This allows for various implementations with different weights on the resulting pitch and heading movement. Furthermore, we show that the algorithm is suitable for vehicles with limitations on the pitch angle, which is the case for many AUVs and UAVs alike.

The remainder of this paper is organized as follows. In Section II we give a brief introduction to some of the mathematical concepts used in the paper. The vehicle and the obstacle model are described in Section III, which also states the sensor requirements and the control objective of the system. Section IV defines the heading and pitch controllers, as well as the guidance laws employed to steer the vehicle towards a target when it is not in CA mode. Section V describes the CA algorithm, which is analyzed in Section VI. The analysis is validated by simulations in Section VII. Finally, concluding remarks and thoughts on future work are given in Section VIII.

II. MATHEMATICAL PRELIMINARIES

Throughout this paper we will use various reference frames. A point p and vector $\boldsymbol{v}$ in reference frame a is denoted p^a and $\boldsymbol{v}^a$, respectively. The rotation matrix from reference frame a to a frame b is denoted $\boldsymbol{R}_a^b$, so that $\boldsymbol{v}^b = \boldsymbol{R}_a^b \boldsymbol{v}^a$.

We decompose a rotation between reference frames into three principal rotations using the Euler angles φ (roll), θ (pitch) and ψ (yaw) [22]. Using the zyx-convention, we define the rotation matrix $\boldsymbol{R}_{zyx}(\varphi, \theta, \psi)$ as

$$\boldsymbol{R}_{zyx} \triangleq \begin{bmatrix} c_\psi c_\theta & -s_\psi c_\varphi + c_\psi s_\theta s_\varphi & s_\psi s_\varphi + c_\psi c_\varphi s_\theta \\ s_\psi c_\theta & c_\psi c_\varphi + s_\varphi s_\theta s_\psi & -c_\psi s_\varphi + s_\theta s_\psi c_\varphi \\ -s_\theta & c_\theta s_\varphi & c_\theta c_\varphi \end{bmatrix}, \quad (1)$$

where c_ψ and s_ψ denote $\cos(\psi)$ and $\sin(\psi)$, respectively. For convenience, we also define the rotation matrices $\boldsymbol{R}_{zy}(\theta, \psi) \triangleq \boldsymbol{R}_{zyx}(0, \theta, \psi)$ and $\boldsymbol{R}_z(\psi) \triangleq \boldsymbol{R}_{zyx}(0, 0, \psi)$.

We will investigate a vehicle which is controlled by steering the heading and pitch angle, as modeled in Section III-A. To this end, we define functions converting a 3D direction into the corresponding heading and pitch. Hence, for a vector $\boldsymbol{v} = [v_x, v_y, v_z]^T$, we define the functions

$$\Psi(\boldsymbol{v}) = \operatorname{atan2}(v_y, v_x), \quad (2)$$

$$\Theta(\boldsymbol{v}) = -\sin^{-1}\left(\tfrac{v_z}{||\boldsymbol{v}||}\right). \quad (3)$$

Hence, $\boldsymbol{v}$ can be written as

$$\boldsymbol{v} = \boldsymbol{R}_{zy}\left(\Theta(\boldsymbol{v}), \Psi(\boldsymbol{v})\right) \cdot [||\boldsymbol{v}||, 0, 0]^T. \quad (4)$$

III. SYSTEM DESCRIPTION

A. Vehicle model

The vehicle is modeled on the kinematic level using the Euler angles pitch (θ_v) and yaw (ψ_v) to describe the rotation from the body frame b to the North-east-down frame n.

Assumption 1: The vehicle is passively stabilized in roll.

Assumption 2: The body-fixed forward speed u_v and angular velocities in yaw, r_v, and pitch, q_v, are assumed to be directly controlled. The angular velocities are furthermore limited by

$$r_v \in [-r_{\max}, r_{\max}], \quad (5a)$$

$$q_v \in [-q_{\max}, q_{\max}], \quad (5b)$$

where $r_{\max} > 0$ and $q_{\max} > 0$ are constant vehicle parameters.

The vehicle model is then given by the following equations:

$$\dot{\boldsymbol{p}}_{\mathrm{v}}^n = \boldsymbol{R}_b^n(\theta_v, \psi_v)\boldsymbol{\nu}_{\mathrm{v}}^b, \quad (6a)$$

$$\dot{\theta}_v = q_v, \quad (6b)$$

$$\dot{\psi}_v = \tfrac{r_v}{\cos(\theta_v)}, \quad (6c)$$

where $\boldsymbol{p}_{\mathrm{v}}^n$ is the vehicle position in the NED frame, $\boldsymbol{\nu}_{\mathrm{v}}^b = [u_v, 0, 0]^T$ is the vehicle velocity in the body frame and $\boldsymbol{R}_b^n = \boldsymbol{R}_{zy}$. Note that the last two elements of $\boldsymbol{\nu}_{\mathrm{v}}^b$, i.e. the sway and heave velocities, are zero due to nonholonomic constraints on the vehicle.

To avoid a singularity in the heading rate in (6c), we impose a bound on the initial pitch:

Assumption 3: The initial pitch satisfies

$$\theta_v(t_0) \in [\theta_{\min}, \theta_{\max}], \quad (7)$$

where $\theta_{\min} \in (-\pi/2, 0)$ and $\theta_{\max} \in (0, \pi/2)$ are constant design parameters.

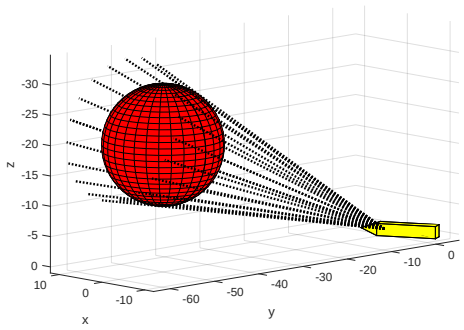

Fig. 1. A sample of rays (dotted black) from the vision cone from the vehicle (yellow) to the obstacle (red).

Remark 1: It is common to impose limits on the maximum and minimum pitch angle of vehicles such as AUVs and many fixed wing aircraft. For AUVs, such limits can increase the vehicle safety by ensuring that it does not move too fast towards the sea floor or the surface. Similarly, aircraft with such limits avoid going too fast towards the ground, and can also avoid stalling scenarios.

Remark 2: Note that the pitch limits do not include zero, in order to ensure that the vehicle is able to move both up and down.

We will design the control system in Section IV and the CA algorithm in Section V in such a way that Assumption 3 ensures that the pitch does not exceed these limits.

We also define the reference frame n_v, which is oriented along the NED frame and which origin coincides with the origin of the body frame. This frame is thus a body-fixed NED frame, and is used to represent the position of the obstacle and the target relative to the vehicle.

B. Obstacle model

The obstacle is modeled as a static, spherical object of radius R_o. The obstacle position in the NED frame is denoted $\boldsymbol{p}_o^n$.

Remark 3: If the obstacle is not spherical, it can be represented using the smallest covering sphere.

C. Sensing model

To implement the proposed CA algorithm, the vehicle must be able to sense the distance d_o between itself and the obstacle. In addition, the vehicle must be able to measure the angles to the edge of the obstacle. These angles define a three-dimensional vision cone $\mathcal{V}_\text{o}$, which is illustrated in Fig. 1. The apex angle of $\mathcal{V}_\text{o}$ is $2\gamma_\text{a}$, where

$$\gamma_\text{a} \triangleq \sin^{-1}\left(\frac{R_\text{o}}{R_\text{o}+d_\text{o}}\right). \tag{8}$$

D. Control objectives

Let $\boldsymbol{p}_\text{t}^n$ be a target position in the NED frame. The objective of the control system and the CA algorithm is to make the vehicle come within an acceptance distance $d_\text{a} \geq u_v/r_\text{max}$ of the target position $\boldsymbol{p}_\text{t}^n$ at some unspecified time $t_\text{f} \in [0, \infty)$, i.e.

$$||\boldsymbol{p}_\text{t}^{n_v}(t_\text{f})|| \leq d_\text{a}, \tag{9}$$

where $\boldsymbol{p}_\text{t}^{n_v} = \boldsymbol{p}_\text{t}^n - \boldsymbol{p}_\text{v}^n$ is the target position in the body-fixed NED frame n_v. This goal should be achieved while keeping at least a minimum safety distance d_safe to the obstacle, i.e. the distance d_o between the vehicle and the obstacle should satisfy:

$$d_\text{o}(t) \geq d_\text{safe} > 0 \quad \forall t \in [t_0, t_f]. \tag{10}$$

To accommodate the pitch limitations often encountered in practice as discussed in Remark 1, the control system should bound the vehicle pitch:

$$\theta_v(t) \in [\theta_\text{min}, \theta_\text{max}] \quad \forall t \in [t_0, t_f]. \tag{11}$$

IV. Control System

The control system can be either in guidance mode, where it drives the vehicle towards the target using the guidance laws given in Section IV-B, or in CA mode where it actively avoids an obstacle. In this section we describe the low-level control laws and the guidance laws, while the CA law is described in Section V. The rule for switching between the two modes is given in Section V-C.

A. Flow frame control

We want the vehicle to reach the desired heading ψ_d and pitch θ_d as fast as possible. Hence, we make it turn at the maximum rate towards the desired direction:

$$r(\psi_\text{d}) \triangleq \begin{cases} 0 & \tilde{\psi} = 0, \\ r_\text{max} & \tilde{\psi} \in (-\pi, 0), \\ -r_\text{max} & \tilde{\psi} \in (0, \pi]. \end{cases} \tag{12a}$$

$$q(\theta_\text{d}) \triangleq \begin{cases} 0 & \tilde{\theta} = 0, \\ q_\text{max} & \tilde{\theta} \in (-\pi, 0), \\ -q_\text{max} & \tilde{\theta} \in (0, \pi]. \end{cases} \tag{12b}$$

The heading error variable $\tilde{\psi} \triangleq \psi_v - \psi_\text{d}$ and the pitch error variable $\tilde{\theta} \triangleq \theta_v - \theta_\text{d}$ are chosen to belong to the interval $\tilde{\psi}, \tilde{\theta} \in (-\pi, \pi]$. This ensures that the vehicle always makes the shortest possible turn towards ψ_d and θ_d. The desired heading ψ_d and pitch θ_d are given in Section IV-B when the control system is in guidance mode, and in Section V when the control system is in CA mode.

B. Guidance laws

When the control system is in guidance mode, we choose to use pure pursuit guidance laws [23] for the desired heading and pitch. The heading guidance law is thus chosen as:

$$\psi_\text{dg} \triangleq \Psi(\boldsymbol{p}_\text{t}^{n_v}), \tag{13}$$

where Ψ is defined in (2), and $\psi_\text{dg} \in [0, 2\pi)$ is the desired heading in guidance mode.

The pitch guidance law is saturated to ensure that control objective (11) is met:

$$\theta_\text{dg} = \begin{cases} \theta_\text{max} & \Theta(\boldsymbol{p}_\text{t}^{n_v}) > \theta_\text{max}, \\ \Theta(\boldsymbol{p}_\text{t}^{n_v}) & \Theta(\boldsymbol{p}_\text{t}^{n_v}) \in [\theta_\text{min}, \theta_\text{max}], \\ \theta_\text{min} & \Theta(\boldsymbol{p}_\text{t}^{n_v}) < \theta_\text{min}, \end{cases} \tag{14}$$

where Θ is defined in (3), and $\theta_\text{dg} \in [\theta_\text{min}, \theta_\text{max}]$ is the desired pitch. If $\Theta(\boldsymbol{p}_\text{t}^{n_v}) \notin [\theta_\text{min}, \theta_\text{max}]$, the guidance law

will drive the vehicle towards the target at maximum or minimum pitch, and then make the vehicle circle up or down until $||\boldsymbol{p}_{\mathrm{t}}^{n_v}(t_{\mathrm{f}})|| \leq d_{\mathrm{a}}$, and control objective (9) is met.

The desired velocity vector in guidance mode, $\boldsymbol{v}_{\mathrm{dg}}^{n_v}$, is then found from the guidance laws (13) and (14) as:

$$\boldsymbol{v}_{\mathrm{dg}}^{n_v} \triangleq \boldsymbol{R}_{zy}(\theta_{\mathrm{dg}}, \psi_{\mathrm{dg}})\boldsymbol{\nu}_{\mathrm{v}}^{b}, \tag{15}$$

where $\boldsymbol{\nu}_{\mathrm{v}}^{b} = [u_v, 0, 0]^T$ as in Section III-A.

V. COLLISION AVOIDANCE ALGORITHM

In this section we define the CA algorithm. In Section V-A we give the mathematical definiton of the algorithm in general terms, while in Section V-B we provide an example implementation. Finally, in Section V-C we give the rule for deciding when the vehicle should enter and exit CA mode.

A. Algorithm definition

The CA algorithm is based on keeping a constant avoidance angle to the obstacle. To this end, the vision cone $\mathcal{V}_{\mathrm{o}}$ is extended by increasing the apex angle by $2\alpha_{\mathrm{o}}$, where $\alpha_{\mathrm{o}} \in [0, \pi/2)$ is a constant design parameter. The apex angle of the extended vision cone $\mathcal{V}_{\mathrm{e}}$ is then $2\gamma_{\mathrm{e}}$, where γ_{e} is

$$\gamma_{\mathrm{e}} \triangleq \gamma_{\mathrm{a}} + \alpha_{\mathrm{o}}. \tag{16}$$

The extended vision cone is illustrated in Fig. 2.

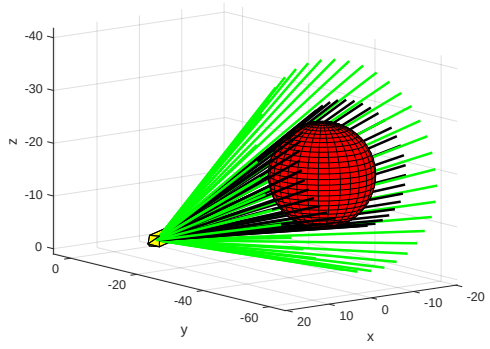

Fig. 2. The extended vision cone (green) from the vehicle to the obstacle.

To safely avoid the obstacle, the vehicle should aim along one of the rays of the extended vision cone. Hence there is a continuum of candidates for the desired heading and pitch during collision avoidance. This is unlike the two-dimensional CA algorithm in [20], which provides only two heading candidates, one to either side of the obstacle. The three-dimensional case thus gives us added flexibility. We will utilize this flexibility and make an optimal choice of which ray along $\mathcal{V}_{\mathrm{e}}$ the vehicle should follow.

To achieve this, we parametrize the directions along $\mathcal{V}_{\mathrm{e}}$ using a parameter ϕ, and define two continuous functions $\psi_{V_e}(\phi)$ and $\theta_{V_e}(\phi)$ to be the vehicle heading and pitch along the ray defined by ϕ. We also define the variables $\tilde{\psi}_{V_e}(\phi)$ and $\tilde{\theta}_{V_e}(\phi)$ as

$$\tilde{\psi}_{V_e}(\phi) \triangleq \psi_v - \psi_{V_e}(\phi), \qquad \tilde{\psi}_{V_e}(\phi) \in (-\pi, \pi], \tag{17a}$$

$$\tilde{\theta}_{V_e}(\phi) \triangleq \theta_v - \theta_{V_e}(\phi), \qquad \tilde{\theta}_{V_e}(\phi) \in (-\pi, \pi]. \tag{17b}$$

These variables represent the difference between the current vehicle direction and the direction of each ray along $\mathcal{V}_{\mathrm{e}}$, and are collected in the error vector $\boldsymbol{e}_{V_e}(\phi) \triangleq [\tilde{\psi}_{V_e}(\phi), \tilde{\theta}_{V_e}(\phi)]^T$.

We let the cost for choosing a direction along $\mathcal{V}_{\mathrm{e}}$ be represented by some cost function $C(\boldsymbol{e}_{V_e}(\phi))$. The cost function is required to be strictly increasing in the norm of $\boldsymbol{e}_{V_e}$, to ensure that the vehicle chooses the closest direction in some sense. Furthermore, the value of C for any $\theta_v \notin [\theta_{\min}, \theta_{\max}]$ is required to be higher than the value of C for any $\theta_v \in [\theta_{\min}, \theta_{\max}]$, in order to give a higher cost to any desired directions violating control objective (11).

To avoid the obstacle, we make the vehicle follow the direction along $\mathcal{V}_{\mathrm{e}}$ which minimizes $C(\boldsymbol{e}_{V_e}(\phi))$. We denote the parameter of this direction ϕ_{ca}, which is defined as:

$$\phi_{\mathrm{ca}} \triangleq \arg\min_{\phi} C(\boldsymbol{e}_{V_e}(\phi)) \tag{18}$$

The desired heading and pitch in collision avoidance are then

$$\psi_{\mathrm{dca}} \triangleq \psi_{V_e}(\phi_{\mathrm{ca}}), \tag{19a}$$

$$\theta_{\mathrm{dca}} \triangleq \theta_{V_e}(\phi_{\mathrm{ca}}). \tag{19b}$$

B. Implementation

It is possible to design the cost function C and parametrization ϕ in several ways, to accommodate any vehicle- or scenario-specific limitations or preferences. We will now present one parametrization $\hat{\phi}$ of $\mathcal{V}_{\mathrm{e}}$, as well as a cost function $\hat{C}$.

To get the heading and pitch angle required by the vehicle to follow a ray ρ along $\mathcal{V}_{\mathrm{e}}$, we will find the direction of ρ in the n_v frame. For convenience, we will first find the direction in a body-fixed reference frame, b_{vo}. This frame is created by rotating the n_v frame so that the x-axis of the b_{vo} frame points along the vehicle-obstacle line. In other words, a unit vector pointing from the vehicle to the obstacle is given in the n_v frame as

$$\boldsymbol{u}_{\mathrm{o}}^{n_v} = \boldsymbol{R}_{zyx}(0, \theta_{vo}, \psi_{vo})\boldsymbol{u}_x, \tag{20}$$

where $\theta_{vo} \triangleq \Theta(\boldsymbol{p}_o^{n_v})$, $\psi_{vo} \triangleq \Psi(\boldsymbol{p}_o^{n_v})$, $\boldsymbol{p}_o^{n_v}$ is the position of the obstacle in the n_v frame and $\boldsymbol{u}_x \triangleq [1, 0, 0]^T$. We let the parameter $\hat{\phi}$ describe a rotation of a ray $\hat{\phi} \in [0, 2\pi)$ radians around the x-axis of b_{vo}. Thus, since the x-axis of b_{vo} is the symmetry axis of $\mathcal{V}_{\mathrm{e}}$, a unit vector along a ray ρ is given in the b_{vo} frame as

$$\boldsymbol{u}_{\rho}^{b_{vo}}(\hat{\phi}) \triangleq \boldsymbol{R}_{zyx}(\hat{\phi}, 0, 0)\boldsymbol{R}_z(\gamma_{\mathrm{e}})\boldsymbol{u}_x. \tag{21}$$

When $\boldsymbol{u}_{\rho}^{b_{vo}}(\hat{\phi})$ is decomposed in the n_v frame, we obtain

$$\begin{aligned} \boldsymbol{u}_{\rho}^{n_v}(\hat{\phi}) &= \boldsymbol{R}_{zyx}(0, \theta_{vo}, \psi_{vo})\boldsymbol{R}_{zyx}(\hat{\phi}, 0, 0)\boldsymbol{R}_z(\gamma_{\mathrm{e}})\boldsymbol{u}_x \\ &= \boldsymbol{R}_{zyx}(\hat{\phi}, \theta_{vo}, \psi_{vo})\boldsymbol{R}_z(\gamma_{\mathrm{e}})\boldsymbol{u}_x. \end{aligned} \tag{22}$$

A vehicle, an obstacle and four rays of $\mathcal{V}_{\mathrm{e}}$ are shown in the b_{vo} frame in Fig. 3. The heading and pitch required by the vehicle to follow each ray are then

$$\psi_{V_e}(\hat{\phi}) = \Psi(\boldsymbol{u}_{\rho}^{n_v}(\hat{\phi})), \tag{23a}$$

$$\theta_{V_e}(\hat{\phi}) = \Theta(\boldsymbol{u}_{\rho}^{n_v}(\hat{\phi})). \tag{23b}$$

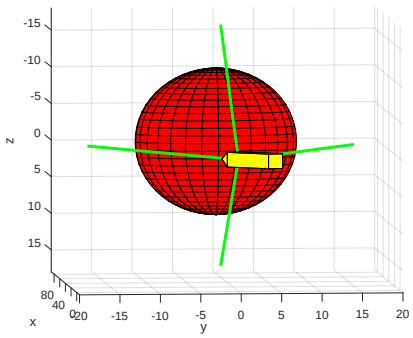

Fig. 3. A vehicle and an obstacle in the b_{vo} frame. The green lines are rays of $\mathcal{V}_\text{e}$, corresponding to $\hat{\phi} = 0$ (right), $\hat{\phi} = \pi/2$ (down), $\hat{\phi} = \pi$ (left) and $\hat{\phi} = 3\pi/2$ (up).

As cost function $\hat{C}$, we define

$$\hat{C} \triangleq \begin{cases} |e_{V_e}|_\infty & \theta_{V_e} \in [\theta_\text{min}, \theta_\text{max}], \\ |e_{V_e}|_\infty + 2\pi & \theta_{V_e} \notin [\theta_\text{min}, \theta_\text{max}]. \end{cases} \tag{24}$$

Using this cost function to find ψ_dca and θ_dca (19) will minimize the maximum amount of vertical or horizontal control effort required, and will tend to make the vehicle use both its control inputs to avoid the obstacle while at the same time ensuring that the pitch stays within limit.

C. Switching rule

We define that the vehicle enters CA mode at a time t_1 if the obstacle is closer than or equal to a chosen range, d_switch, and the desired velocity vector $\boldsymbol{v}_\text{dg}^{n_v}(t_1)$ (15) from the nominal guidance laws (13) and (14) is within the extended vision cone $\mathcal{V}_\text{e}(t_1)$:

$$\boldsymbol{v}_\text{dg}^{n_v}(t_1) \in \mathcal{V}_\text{e}(t_1), \tag{25a}$$

$$d_\text{o}(t_1) \leq d_\text{switch} \in (d_\text{safe}, d_\text{sense}]. \tag{25b}$$

Nominal guidance towards the target will resume at a time t_2 when $\boldsymbol{v}_\text{dg}^{n_v}(t_2)$ moves outside $\mathcal{V}_\text{e}(t_2)$:

$$\psi_\text{dg}(t_2) \notin \mathcal{V}_\text{e}(t_2). \tag{26}$$

VI. ANALYSIS

In this section we give an analysis of the CA algorithm presented in Section V, applied to the vehicle described by the model given in (6). The vehicle model is in closed loop configuration with the heading and pitch controllers (12). The vehicle is nominally moving towards a target position $\boldsymbol{p}_\text{t}^n$ using the guidance laws (13) and (14). When the vehicle encounters an obstacle, it switches into CA mode using the switching criterion in Section V-C, and follows the heading and pitch reference given by (19) to avoid the obstacle.

We will in particular derive bounds on the switching distance d_switch in (25) and on the avoidance angle α_o in (16), which guarantee that the control objectives in Section III-D are met.

A. Safety distance

We start by showing that by a proper choice of the avoidance angle α_o, we can guarantee that when the vehicle follows the heading and pitch references (19) of the CA law, the vehicle maintains at least the minimum safety distance d_safe from the obstacle.

Lemma 1: If

$$\alpha_\text{o} \geq \cos^{-1}\left(\frac{R_\text{o}}{R_\text{o}+d_\text{safe}}\right), \tag{27}$$

the initial obstacle distance $d_\text{o}(t_0) \geq d_\text{safe}$, and the vehicle follows the CA heading law (19a) and pitch law (19b), then

$$d_\text{o}(t) \geq d_\text{safe} \quad \forall t \geq t_0. \tag{28}$$

Proof: When the vehicle follows one of the rays of the extended vision cone, the time derivative of the distance d_o between the vehicle and the obstacle can be found geometrically:

$$\dot{d}_\text{o}(t) = -u_v \cos(\gamma_\text{a}(t) + \alpha_\text{o}) \tag{29}$$

$$= -u_v \cos\left(\sin^{-1}\left(\frac{R_\text{o}}{R_\text{o}+d_\text{o}(t)}\right) + \alpha_\text{o}\right). \tag{30}$$

The obstacle distance is constant when $\gamma_\text{a}(t) + \alpha_\text{o} = \pi/2$, which occurs when

$$d_\text{o}(t) = \bar{d} \triangleq \frac{R_\text{o}}{\cos(\alpha_\text{o})} - R_\text{o}. \tag{31}$$

When $d_\text{o}(t) < \bar{d}$, $\dot{d}_\text{o}(t) > 0$, while when $d_\text{o}(t) > \bar{d}$, $\dot{d}_\text{o}(t) < 0$. It follows that if $d_\text{safe} = \bar{d}$ and $d_\text{o}(t_0) \geq d_\text{safe}$, then a vehicle following (19a) and (19b) perfectly will not get closer than d_safe to the obstacle. ■

B. Safe avoidance

We now show that if the vehicle is aligned with the extended vision cone at some time t_2, then it is guaranteed to be safe as long as it is in CA mode.

Lemma 2: Consider a vehicle modeled by (6) and governed by the controllers (12), the guidance laws (13) and (14) and the CA laws (19). Let there exist a time t_2 when the vehicle is in CA mode, $d_\text{o}(t_2) \geq d_\text{safe}$, $\psi_v(t_2) = \psi_\text{dca}$ and $\theta_v(t_2) = \theta_\text{dca}$. Finally, let there be a time $t_3 > t_2$ at which the vehicle exits CA mode. Then, the distance to the obstacle satisfies

$$d_\text{o}(t) \geq d_\text{safe} \quad \forall t \in [t_2, t_3]. \tag{32}$$

Proof: When $\tilde{\psi} = 0$ and $\tilde{\theta} = 0$, the vehicle is oriented along a ray $\bar{\rho}$ of the extended vision cone $\mathcal{V}_\text{e}$. For clarity, we observe the system in a plane $\bar{P}$ containing $\bar{\rho}$, the obstacle center and the vehicle. The system observed in this plane is illustrated in Fig. 4. The angle from the x-axis to $\bar{\rho}$ is denoted β, and can be decomposed into

$$\beta = \gamma_\text{o} + \gamma_\text{a} + \alpha_0. \tag{33}$$

Here, γ_o is the angle from the x-axis to the vehicle-obstacle line, and γ_a is the angle from this line to the vision cone $\mathcal{V}_\text{o}$ from the vehicle to the obstacle. By construction, the x-axis of the vehicle's body frame b, denoted x^b in the figure, lies in $\bar{P}$, and the rotation angle from $\bar{P}$ to b is denoted $\bar{\psi}$, as shown in Fig. 4.

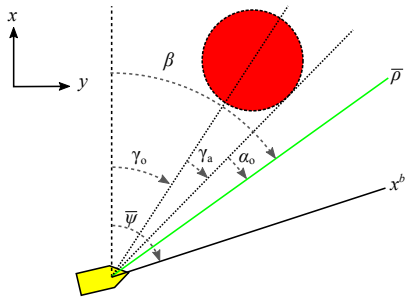

Fig. 4. The vehicle and the obstacle in the plane $\bar{P}$ containing the ray $\bar{\rho}$ and the obstacle center.

It follows from (33) that

$$\dot{\beta} = \dot{\gamma}_o + \dot{\gamma}_a. \tag{34}$$

The angular velocity of γ_o can be found geometrically as

$$\dot{\gamma}_o = -\frac{u_v}{R_o+d_o}\sin(\bar{\psi}-\gamma_o). \tag{35}$$

The tangent angle γ_a is

$$\gamma_a = \sin^{-1}\left(\frac{R_o}{R_o+d_o}\right), \tag{36}$$

which gives

$$\dot{\gamma}_a = -\dot{d}_o \frac{R_o}{(R_o+d_o)\sqrt{(R_o+d_o)^2-R_o^2}}, \tag{37}$$

where time derivative of d_o is

$$\dot{d}_o = -u_v\cos(\bar{\psi}-\gamma_o). \tag{38}$$

We define the error variable $\bar{\psi}_e$ as

$$\bar{\psi}_e = \bar{\psi} - \beta. \tag{39}$$

By combining (35) and (37), and inserting for $\bar{\psi} = \bar{\psi}_e + \beta$, we obtain the dynamics of $\bar{\psi}_e$:

$$\dot{\bar{\psi}}_e = \bar{r} + \frac{u_v\sin(\bar{\psi}_e+\alpha_0)}{\sqrt{(R_o+d_o)^2-R_o^2}}, \tag{40}$$

where $\bar{r} \triangleq \dot{\bar{\psi}}$, which is set by the controllers in (12). When $\bar{\psi}_e = 0$, $\dot{\bar{\psi}}_e$ becomes

$$\dot{\bar{\psi}}_e = \bar{r} + \frac{u_v\sin(\alpha_0)}{\sqrt{(R_o+d_o)^2-R_o^2}}. \tag{41}$$

The $\dot{\beta}$ term is then positive since $\alpha_0 \in (0, \frac{\pi}{2})$. The value of $\bar{r}$ lies in the interval $[-\bar{r}_{\max}, \bar{r}_{\max}]$, where $\bar{r}_{\max}$ is found from (12) as

$$\bar{r}_{\max} \triangleq \sqrt{r_{\max}^2 + q_{\max}^2}. \tag{42}$$

If $\dot{\beta} > \bar{r}_{\max}$, it follows from (41) that $\dot{\bar{\psi}}_e > 0$. Hence, the vehicle direction will drift away from the extended vision cone $\mathcal{V}_e$. Lemma 1 implies that as long as the vehicle maintains a direction of $\mathcal{V}_e$, it will never come closer than the distance d_{safe} to the obstacle. This can be seen from Figure 4, where it is clear that a direction outside of $\bar{\rho}$ will lead the vehicle further away from the obstacle than following $\bar{\rho}$.

The implementation of the cost function $C(\boldsymbol{e}_{V_e}(\phi))$ in Section V can make the desired direction from collision avoidance move away from the plane $\bar{P}$. In this case, since the obstacle is convex, the vehicle direction will still glide away from $\mathcal{V}_e$. Hence, as long as there is a time t_2 when the vehicle is aligned with a ray of $\mathcal{V}_e$, the vehicle distance is guaranteed to be greater than d_{safe} while the vehicle is in CA mode. ■

Remark 4: To get an intuitive understanding of Lemma 2, consider a case where the vehicle is aligned with a ray along the extended vision cone $\mathcal{V}_e$, and never turns. The vehicle will then continue in a straight line, past the obstacle.

C. Safe navigation

This section contains the main theorem of the paper, which states that the vehicle will safely reach the target when navigating an environment containing an obstacle. Before we state the theorem, we make the assumptions that the vehicle is able to start safely, and that the obstacle does not cover the target.

Assumption 4: The initial distance between the vehicle and the obstacle satisfies

$$d_o(t_0) > d_{\text{switch}}. \tag{43}$$

Assumption 5: The distance $d_{o,t}(t)$ from the obstacle to the target position $\boldsymbol{p}_t^n$ satisfies

$$d_{o,t}(t) > \frac{R_o}{\cos(\alpha_o)} - R_o \tag{44}$$

Remark 5: Vehicle safety is guaranteed even if this assumption is not met, however it is then not ensured that the target will be reached.

Theorem 1: Let Assumptions 1-5 hold, the avoidance angle α_o satisfy

$$\alpha_o \in \left[\cos^{-1}\left(\frac{R_o}{R_o+d_{\text{safe}}}\right), \frac{\pi}{2}\right), \tag{45}$$

and the switching distance satisfy

$$d_{\text{switch}} \geq \frac{u_v}{r_{\max}} + d_{\text{safe}}. \tag{46}$$

Furthermore, let the vehicle be modeled by (6) and governed by the controllers (12), the guidance laws (13) and (14) and the CA laws (19). Then, there exists a time $t_f \geq t_0$ such that

$$||\boldsymbol{p}_t^{n_v}(t_f)|| \leq d_a. \tag{47}$$

Moreover,

$$d_o(t) \geq d_{\text{safe}} \quad \forall t \in [t_0, t_f], \tag{48}$$

and

$$\theta_v(t) \in [\theta_{\min}, \theta_{\max}] \quad \forall t \in [t_0, t_f]. \tag{49}$$

Hence, the control objectives (9), (10) and (11) are met.

Proof: Consider a time $t_1 \geq t_0$, at which the vehicle enters CA mode in accordance with (25). The vehicle then chooses a direction which minimizes the cost function C, and starts to turn towards this direction at the maximum yaw rate $r_{\max}$ and pitch rate $q_{\max}$.

In a worst case scenario, where the bounds on the vehicle pitch makes the vehicle take the entire turn horizontally, the change in yaw required by the vehicle to avoid the obstacle is upper bounded by $\pi/2$ rad. The radius of a horizontal turning circle of the vehicle is $u_v/r_{\max}$ m. Hence, the vehicle will move a maximum of $u_v/r_{\max}$ m towards the obstacle before reaching the extended vision cone $\mathcal{V}_e$. The minimum

switching distance given by (46) thus ensures that there is a time $t_2 > t_1$ at which the vehicle is aligned with a ray of $\mathcal{V}_\text{e}$, and that

$$d_\text{o}(t) \geq d_\text{safe} \quad \forall t \in [t_0, t_2]. \tag{50}$$

At time t_2, the conditions of Lemma 2 are met. Hence, the obstacle distance will not be less than d_safe until a time $t_3 > t_2$, when the direction towards the target comes outside $\mathcal{V}_\text{e}$. The switching rule in Section V-C gives that the control system now enters guidance mode. Lemma 1 implies that moving in a direction outside of $\mathcal{V}_\text{e}$ will never lead the vehicle closer than d_safe to the obstacle. Thus it is ensured that condition (48) is fulfilled.

The guidance laws in (13) and (14) steer the vehicle towards the target at maximum turning rate. Hence, it is ensured that there exist a time t_f when $||\boldsymbol{p}_\text{t}^{n_v}(t_\text{f})|| \leq d_\text{a}$, fulfilling condition (47).

As long as $\theta_v(t_0) \in [\theta_\text{min}, \theta_\text{max}]$ and $\theta_\text{d} \in [\theta_\text{min}, \theta_\text{max}]$, Assumption 2 and the pitch control law (12b) ensures that $\theta_\text{dg} \in [\theta_\text{min}, \theta_\text{max}]$ $\forall t \in [t_0, t_f]$. While the definition of C ensures that $\theta_\text{dca} \in [\theta_\text{min}, \theta_\text{max}]$, the definition of the pitch guidance law (14) ensures that $\theta_\text{dg} \in [\theta_\text{min}, \theta_\text{max}]$. Thus, $\theta_\text{d} \in [\theta_\text{min}, \theta_\text{max}]$ $\forall t \in [t_0, t_f]$, and Assumption 3 ensures that condition (49) is fulfilled. ■

Remark 6: Note that this proof also holds for a scenario with multiple, consecutive obstacles. The condition then would be that the inter-obstacle distance are at least $2d_\text{switch}$, so that each obstacle is avoided separately.

VII. Simulations

In this section we will present numerical simulations to validate the analysis in Section VI. The simulations use the parametrization $\hat{\phi}$ and cost function $\hat{C}$ presented i Section V-B. The simulation parameters used in the simulations are summarized in Table I.

TABLE I
Simulation parameters

r_max	$0.1\,\text{rad/s}$	θ_min	$-25\,^\circ$
q_max	$0.1\,\text{rad/s}$	θ_max	$25\,^\circ$
u_v	$2\,\text{m/s}$	$\boldsymbol{p}_\text{v}^n(t_0)$	$[0,0,0]^T$ (m)
R_o	$10\,\text{m}$	$\boldsymbol{p}_\text{t}^n(t_0)$	$[150,0,0]^T$ (m)
d_safe	$5\,\text{m}$	d_a	$20\,\text{m}$

The avoidance angle α_o was set using (45) to $41.4\,^\circ$, while the switching distance was set using (46) to d_switch= $25\,\text{m}$.

The obstacle position was set to $\boldsymbol{p}_o^n = [70, y_\text{o,sim}, z_\text{o,sim}]^T$ (m), where $y_\text{o,sim}$ and $z_\text{o,sim}$ were set to increase incrementally from $-15\,\text{m}$ to $15\,\text{m}$ in steps of $1\,\text{m}$ for each simulation, creating a set of 961 simulations. The results of the simulations are summarized in Table II, where $d_\text{o,min}$ denotes the minimum obstacle distance during a simulation, $\theta_\text{v,min}$ denotes the minimum pitch during a simulation, while $\theta_\text{v,max}$ denotes the maximum pitch value.

The results in Table II verify the results of Theorem 1 in that the vehicle always reaches the target, the safety distance is never violated and the bounds on θ_v are upheld.

TABLE II
Simulation results

Min $d_\text{o,min}$	$7.3\,\text{m}$	Min $t_\text{f} - t_0$	$65.3\,\text{s}$
Max $d_\text{o,min}$	$14.6\,\text{m}$	Max $t_\text{f} - t_0$	$69.6\,\text{s}$
Min $\theta_\text{v,min}$	$-25\,^\circ$	Min $\theta_\text{v,max}$	$1.7\,^\circ$
Max $\theta_\text{v,min}$	$-1.7\,^\circ$	Max $\theta_\text{v,max}$	$25\,^\circ$

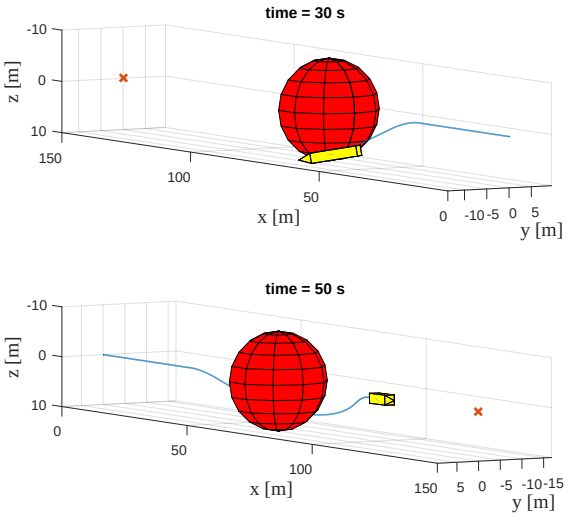

Fig. 5. A scenario where the obstacle is straight ahead of the vehicle. The vehicle is the yellow polyhedron, and the obstacle is the red sphere. The blue line is the vehicle trajectory, while the target is marked by an 'X'.

An example scenario is shown in Fig. 5, where $y_\text{o,sim} = z_\text{o,sim} = 0\,\text{m}$. The obstacle is thus straight ahead of the vehicle, and there are four possible direction minimizing $\hat{C}$; to the upper or lower right, and to the upper or lower left. The choice becomes random, and in this case the vehicle moves towards the lower left. The pitch is limited by θ_min, and the maneuver is dominated by horizontal movement. When the line of sight to the target comes outside $\mathcal{V}_\text{e}$, the vehicle exits CA mode and continues under nominal guidance.

Another example is shown in Figure. 6, where $y_\text{o,sim} = 4\,\text{m}$ and $z_\text{o,sim}$ $5\,\text{m}$. The direction along $\mathcal{V}_\text{e}$ minimizing $\hat{C}$ is then to the upper left of the vehicle. The pitch is now limited by θ_max. The vehicle proceeds towards the target under nominal guidance once the vehicle-target line comes outside of $\mathcal{V}_\text{e}$.

VIII. Conclusions and Future Work

This paper has presented a 3D reactive collision avoidance algorithm for nonholonomic vehicles. During the collision avoidance maneuver, the algorithm makes the vehicle keep a constant avoidance angle to the obstacle by steering the vehicle heading and pitch. The algorithm includes bounds on the allowed vehicle pitch, and ensures that they are upheld. Such bounds are commonly seen in real life scenarios involving, for example, fixed wing aircraft or AUVs. Furthermore, a general optimality criterion has been presented for choosing an optimal, in some sense, safe vehicle direction. Thus, it

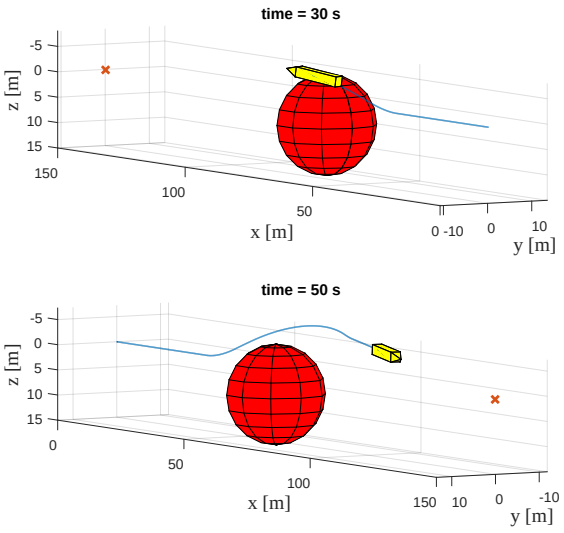

Fig. 6. A scenario where $y_{\text{o,sim}} = 4\,\text{m}$ and $z_{\text{o,sim}}$ $5\,\text{m}$.

is possible to implement different weights on horizontal and vertical turning maneuvers, and it is possible to implement costs to comply with any rules of the road.

The main theorem of the paper states the minimum distance before the obstacle the vehicle needs to start to turn in order to ensure collision avoidance, and gives the minimum required avoidance angle the vehicle must keep to the obstacle in order to stay at least a minimum distance away from it. The results are verified by several simulations.

While the work in this paper only considers a single obstacle, it is possible to extend it to a multi-obstacle scenario. The mathematical analysis holds for a sparse scenario where the vehicle only needs to consider one obstacle at a time. For a more dense scenario, the extended vision cones for the obstacles within range must be merged. Implementing and analyzing such a scenario is a topic for future work.

The obstacle considered in this paper has been assumed to be static. A natural next step in the development of the presented algorithm is to include dynamic obstacles. A multiagent scenario with other agents employing the same algorithm is also of interest. In such a case, the function for choosing a safe direction can be augmented to include rules of the road. Finally, a topic for future research will be to incorporate a more complete vehicle model. This can include underactuated dynamics, which can give the vehicle underactuated velocity components in addition to the directly controlled forward speed.

REFERENCES

[1] T. Statheros, G. Howells, and K. M. Maier, "Autonomous Ship Collision Avoidance Navigation Concepts, Technologies and Techniques," *Journal of Navigation*, vol. 61, no. 01, pp. 129–142, 2008.

[2] M. Hoy, A. S. Matveev, and A. V. Savkin, "Algorithms for collision-free navigation of mobile robots in complex cluttered environments: a survey," *Robotica*, vol. 33, no. 03, pp. 463–497, 2014.

[3] L. Lapierre, R. Zapata, and P. Lepinay, "Combined path-following and obstacle avoidance control of a wheeled robot," *The International Journal of Robotics Research*, vol. 26, no. 4, pp. 361–375, 2007.

[4] J. Canny and J. Reif, "New lower bound techniques for robot motion planning problems," in *Proc. 28th Annual Symposium on Foundations of Computer Science*, (Los Angeles, CA, USA), pp. 49–60, 1987.

[5] O. Khatib, "Real-time obstacle avoidance for manipulators and mobile robots," *The International Journal of Robotics Research*, vol. 5, no. 1, pp. 90–98, 1986.

[6] Y. Koren and J. Borenstein, "Potential field methods and their inherent limitations for mobile robot navigation," in *Proc. IEEE International Conference on Robotics and Automation (ICRA)*, (Sacramento, CA, USA), pp. 1398–1404, 1991.

[7] J. Borenstein and Y. Koren, "The vector field histogram–Fast obstacle avoidance for mobile robots," *IEEE Transactions on Robotics and Automation*, vol. 7, no. 3, pp. 278–288, 1991.

[8] D. Panagou, "Motion planning and collision avoidance using navigation vector fields," in *Proc. IEEE International Conference on Robotics & Automation (ICRA)*, (Hong Kong, China), pp. 2513–2518, 2014.

[9] D. Fox, W. Burgard, and S. Thrun, "The dynamic window approach to collision avoidance," *IEEE Robotics and Automation Magazine*, vol. 4, no. 1, pp. 23–33, 1997.

[10] B. O. H. Eriksen, M. Breivik, K. Y. Pettersen, and M. S. Wiig, "A modified dynamic window algorithm for horizontal collision avoidance for AUVs," in *Proc. 2016 IEEE Conference on Control Applications (CCA)*, (Buenos Aires, Brazil), pp. 499–506, 2016.

[11] G. Roussos, D. V. Dimarogonas, and K. J. Kyriakopoulos, "3D navigation and collision avoidance for nonholonomic aircraft-like vehicles," *International Journal of Adaptive Control and Signal Processing*, vol. 24, pp. 900–920, 2010.

[12] P. Fiorini and Z. Shiller, "Motion planning in dynamic environments using velocity obstacles," *The International Journal of Robotics Research*, vol. 17, no. 7, pp. 760–772, 1998.

[13] A. Chakravarthy and D. Ghose, "Obstacle avoidance in a dynamic environment: A collision cone approach," *IEEE Transactions on Systems, Man, and Cybernetics Part A:Systems and Humans.*, vol. 28, no. 5, pp. 562–574, 1998.

[14] D. Wilkie, J. Van Den Berg, and D. Manocha, "Generalized velocity obstacles," in *Proc. IEEE/RSJ International Conference on Intelligent Robots and Systems,*, (St. Louis, MA, USA), pp. 5573–5578, 2009.

[15] J. van den Berg, J. Snape, S. J. Guy, and D. Manocha, "Reciprocal collision avoidance with acceleration-velocity obstacles," in *Proc. IEEE International Conference on Robotics and Automation (ICRA 2011)*, (Shanghai, China), pp. 3475–3482, 2011.

[16] Y. I. Jenie, E.-J. Van Kampen, C. C. de Visser, J. Ellerbroek, and J. M. Hoekstra, "Three-Dimensional Velocity Obstacle Method for UAV Deconflicting Maneuvers," in *Proc. AIAA Guidance, Navigation, and Control Conference*, (Kissimmee, FL, USA), 2015.

[17] Y. I. Jenie, E.-J. van Kampen, C. C. de Visser, J. Ellerbroek, and J. M. Hoekstra, "Three-Dimensional Velocity Obstacle Method for Uncoordinated Avoidance Maneuvers of Unmanned Aerial Vehicles," *Journal of Guidance, Control, and Dynamics*, vol. 39, no. 10, pp. 2312–2323, 2016.

[18] A. V. Savkin and C. Wang, "A simple biologically inspired algorithm for collision-free navigation of a unicycle-like robot in dynamic environments with moving obstacles," *Robotica*, vol. 31, no. 6, pp. 993–1001, 2013.

[19] C. Wang, A. V. Savkin, and M. Garrett, "A Strategy for Safe 3D Navigation of Non-Holonomic Under-Actuated Robots among Moving Obstacles," *Robotica*, vol. 36, no. 2, pp. 275–927, 2018.

[20] M. S. Wiig, K. Y. Pettersen, and A. V. Savkin, "A reactive collision avoidance algorithm for nonholonomic vehicles," in *Proc. 1st IEEE Conference on Control Technology and Applications*, (Kona, HI, USA), 2017.

[21] M. S. Wiig, K. Y. Pettersen, and T. R. Krogstad, "A reactive collision avoidance algorithm for vehicles with underactuated dynamics," in *Proc. 56th IEEE Conference on Control Technology and Applications*, (Melbourne, Australia), 2017.

[22] T. I. Fossen, *Handbook of marine craft hydrodynamics and motion control*. John Wiley & Sons, 2011.

[23] M. Breivik and T. I. Fossen, "Guidance laws for planar motion control," in *Proc. IEEE Conference on Decision and Control*, (Cancun, Mexico), pp. 570–577, 2008.